Self-assembly via anisotropic interactions

Modeling association kinetics of patchy particle systems and self-assembly induced by critical Casimir forces

Newton, A.C.

Publication date
2017

Document Version
Other version

License
Other

5 The role of multivalency in the self-assembly kinetics of patchy particle complexes

Association and dissociation of particles are elementary steps of many natural and technological relevant processes. For many of such processes the presence of multiple binding sites is essential. For instance, protein complexes and regular structures such as virus shells are formed from elementary building blocks with multiple binding sites. Here we address a fundamental question concerning the role of multivalency of binding sites in the association kinetics of such complexes. Using single replica transition interface sampling simulations, we investigate the influence of the multivalency on the binding kinetics and the association mechanism of patchy particles that form polyhedral clusters. When the individual bond strength is fixed, the kinetics naturally is very dependent on the multivalency, with dissociation rate constants exponentially decreasing with the number of bonds. In contrast, we find that when the total bond energy per particle is kept constant association and dissociation rate constants turn out rather independent of multivalency, although of course very dependent on the total energy. The association and dissociation mechanism, however, depends on the presence and nature of the intermediate states. For instance, pathways that visit intermediate states are less prevalent for particles with five binding sites compared to the case of particles with only three bonds. The presence of intermediate states can lead to kinetic trapping, and malformed aggregates. We discuss implications for natural forming complexes such as virus shells and for the design of artificial colloidal patchy particles.

5.1 Introduction

Particles with multiple binding sites are ubiquitous in natural and synthetic systems. Proteins naturally form complexes by binding via multiple sites, virus shells are assembled from capsid proteins with multiple interactions, and nano structures can be built from multivalent patchy particles. Indeed, breakthroughs in colloid synthesis enable colloids to bind anisotropically via multiple binding sites or patches [4, 5, 16, 17]. Such multivalent patchy colloids can form not only crystal phases, but also lead to chains, lamellar structures, colloidal micellar structures and even colloidal hollow shells that are reminiscent of viral shells.

When complex structures are self-assembling from elementary building blocks, their ground state structure should be both thermodynamically stable and at the same time kinetically accessible [61, 63, 70, 134]. When many building blocks are involved the self assembly usually occurs via multiple intermediate states before reaching the final ground state. Such intermediate structures can be short-lived, but also very long-lived. Long lived intermediates occur typically when non-native bonds are formed, yielding a frustrated intermediate, that can only reach the ground state by breaking those frustrated bonds again. Clearly, such frustrated states can restrict the formation of the ground-state cluster within a viable timeframe, also because such malformed bonds can lead to larger kinetically trapped random aggregates. It is therefore, in fact, rather surprising that in nature certain self-assembly processes are so successful, *e.g.* virus assembly. Indeed, previous studies have shown that the conditions for successful self assembly of multivalent particles rely on a fine tuning of interaction parameters such as the bonding strength or bonding volume [5, 63, 70]. When the interaction strength is too strong there is no binding at all, when too large, the system becomes frustrated. When the bonding volume (patch width) is too narrow, there is no binding, when too wide, the system forms random aggregates. Moreover, there is an important role for non-specific binding interactions, which allows the particles to bind weakly first, before finding the final correct target configuration [21]. These findings are universal self-assembly principles that can lead to rational design rules for artificial molecular or colloidal superstructures.

The question we would like to address here is what role multivalency plays in association and dissociation processes, and what influence it has on the kinetics and mechanism of these processes. Multivalent particles can form multiple bonds with other particles or previously formed complexes, yielding a correctly formed structure, or possibly a malformed intermediate state. How does the formation mechanics and kinetics of correctly formed structures depend on the number of bonds the particles can form? To address this question we study a simple model system of spherical particles with multiple binding sites or patches. In chapter 4 we studied the formation of a tetramer from its four constituent particles with three binding sites [135]. In this chapter we systematically extend this study to particles with four and five binding sites. Such particles, can form symmetrical octahedrons and icosahedrons. Since the number of intermediates rises combinatorially with the number of constituent building blocks we will investigate as a first step the

final assembly process, the association/dissociation of the last particle, which is a uniquely defined step in the assembly as it leads to and from the fully formed symmetric polyhedral cluster. As such, all other particles already in the cluster are constrained. We study three different types of clusters, a tetrahedron, a octahedron and an icosahedron where each particle forms three, four or five bonds, respectively (see Fig. 5.1 for a schematic representation of the clusters). For each of these clusters three conformations are defined: a fully bound (B), an unbound state (U) and a partially bound cluster (I) where certain bonds result in a rotationally frustrated state.

While previous work focused mostly on the thermodynamic stability as well as the kinetic accessibility [21, 61, 70, 136], here we are more concerned with the actual kinetics, the rate constants of assembly and disassembly, and the reactive pathways of association and disassociation. Due to the high binding energies necessary to obtain stable clustered structures from patchy particles, obtaining reactive pathways in a statistically meaningful way by brute force molecular dynamics is extremely inefficient. Recently, path sampling techniques have been developed to solve this problem by biasing the generation of reactive pathways without altering the underlying dynamics. We apply the Single Replica Transition Interface Sampling (SRTIS) framework to study rare association/dissociation events involved in the final steps toward the fully formed polyhedron [104, 108].

By analyzing the rate matrix obtained from SRTIS all kinetic information on the overall association dissociation process can be retrieved. A convenient framework is Transition Path Theory, which gives insight in relevant quantities such as commitment probabilities and the net flux through intermediate states [110]. The multivalency has a trivial way of influencing the thermodynamics of binding and the associated kinetics: for a fixed patch binding interaction the binding equilibrium constant increases exponentially with the number of bonds. When the bond strength is fixed, the kinetics also is very dependent of the multivalency, with dissociation rate constants exponentially decreases with the number of bonds. This makes it hard to study the influence of just the number of binding sites. Therefore, we compare not the individual patch strength, but the total binding strength per particle upon complete binding. Remarkably, when the total bond energy is kept constant, the association and dissociation rate constants are rather independent of multivalency. Of course, the kinetics is very dependent on the total binding energy of all particles. The association and dissociation mechanism however depend on the presence and nature of the intermediate states. Pathways that visit the intermediate states are less prevalent for higher five-fold multivalent particles, compared to particles with only three bonds. Such intermediate states can lead to kinetic trapping, and malformed aggregates. We discuss implications for natural forming complexes such as virus shells.

We show that the intermediates have an effect on the overall association or dissociation process and as such the mechanism. A difference is found between the frequency of visiting intermediate states given by TPT, and the actual residence time in the intermediate state given by the time-evolution of the populations.

The remainder of the chapter is as follows. In section 5.2 we explain the

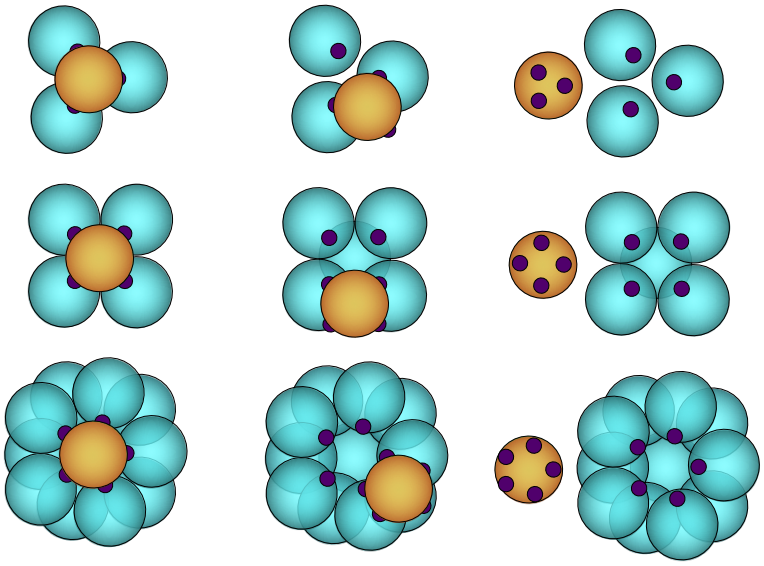

Figure 5.1: Cartoon image of the three polyhedrons considered in this work where the orange particle is the motile particle and the patches are depicted in purple. From top to bottom: tetrahedron, octahedron, icosahedron. From left to right are the three different states: the ground state B, a realization of a frustrated intermediate state I and the unbound state U.

patchy particle model, briefly explain Dynamic Monte Carlo, and end with a small summary of TPT and steady state analysis. In section 5.3 we present the main results of the paper. We end with concluding remarks.

5.2 Methods and Simulation details

Patchy particle model

Similarly to the study of Wilber *et.al.* [61], we use a simple patchy particle model. The potential between particles is defined as:

$$u(\mathbf{r_{ij}}, \Omega_i, \Omega_j) = u_{rep}(\mathbf{r_{ij}}) + u_p(\mathbf{r_{ij}}, \Omega_i, \Omega_j)$$

where $\mathbf{r_{ij}}$ is the inter-particle vector and $\Omega_{i,j}$ the orientations of the particles, stored in quaternion form. The isotropic WCA-like repulsive potential is given by:

$$u_{rep}(\mathbf{r_{ij}}) = \begin{cases} 4.0\left[\left(\frac{\sigma}{r}\right)^{24} - \left(\frac{\sigma}{r}\right)^{12} + \frac{1}{4}\right] & \text{if} \quad r \leq 2^{\frac{1}{12}}\sigma \\ 0 & \text{if} \quad r > 2^{\frac{1}{12}}\sigma \end{cases} \tag{5.1}$$

where $r = |\mathbf{r_{ij}}|$ is the distance between particles, σ determines the size of the particle. The anisotropic patchy interaction is given by:

$$u_p(\mathbf{r_{ij}}, \Omega_i, \Omega_j) = \begin{cases} 4.0\epsilon \left[\left(\frac{\sigma}{r}\right)^{24} - \left(\frac{\sigma}{r}\right)^{12} \right] \mathcal{S}(\mathbf{r_{ij}}, \Omega_i, \Omega_j) & \text{if} \quad r \leq r_c \\ 0 & \text{if} \quad r > r_c \end{cases} \tag{5.2}$$

where ϵ defines the strength of the interaction. We model the interaction between the particles and the patches based on a 24-12 LJ potential. This potential is of shorter range than the standard 12-6 LJ potential. As such the phase behavior exhibits a meta stable liquid vapor coexistence line with respect to the gas solid coexistence [137], similar to protein solutions. The continuous patch function $\mathcal{S}(\Omega_i, \Omega_j)$ gives a penalty for misalignment:

$$\mathcal{S}(\mathbf{r_{ij}}, \Omega_i, \Omega_j) = \exp\left(-\frac{\theta_i^2 + \theta_j^2}{2\delta^2} \right) \tag{5.3}$$

where δ defines the patch-width and θ_α is the angle between patch vectors α and $\mathbf{r_{ij}}/r$ where α is the patch vector which minimizes the angle. Therefore, only the patches on each particle that are closest to $\mathbf{r_{ij}}$ interact. We consider particles with narrow patches ($\delta = 10$ degrees) such that every bond is well defined and there are no multiple overlaps between patches. A small patch-width as used here was shown to reproduce the gas-liquid curves of protein solutions such as γ-crystallin and lysozyme quite well [138], albeit with more patches. Note that this patchy model is somewhat simpler than in chapter 4, as now we no longer require multiple bonds per particle pair.

Dynamics

Overdamped Langevin (Brownian) dynamics are typically used to propagate protein or colloidal systems in time [83, 130]. However, due to the constraint on the immobile particles, the force calculation is rather difficult. Therefore,we use Dynamic Monte Carlo because of the ease of implementation without losing the necessary dynamical information, see section 2.3 [94]. In each DMC cycle a translation and rotation move is tried. A translation move consists of translating a particle by a randomly chosen shift between $[-\delta r, \delta r]$ for each Cartesian axis. A rotation move is done by choosing a random unit vector and rotating the orientation over a randomly chosen angle between $[0, \delta\theta]$. The main disadvantage of DMC is the fact that collective motion of clusters is suppressed [74, 93]. However, collective motion is not important for this system as we only consider one particle to move freely. The rotational and translational step sizes are fixed following the Stokes-Einstein relation, $\delta r = 0.01\sigma$ and $\delta\theta = 0.03$rad, see chapter 2 for more information on DMC.

Single replica Transition Interface Sampling

Single replica transition interface sampling (SRTIS) is used to sample path space and thus obtain the rate matrix [104, 108]. Three states are defined: the fully bound state (B), the unbound state (U) and an intermediate state (I) where two bonds are formed, and the system is frustrated such that the remaining unbound patches are unable to form bonds via barrier-less rotation. When the mobile particle is at least r_U away from the centre of the polyhedron, the system is in the unbound state, where r_U is chosen such that when in U, the mobile particle is at least 2.0σ away from any particle.

The other two states are defined by the correct topology and when the energy of the system is lower than $-0.9n_b\epsilon$ where n_b is the number of bonds that defines the state. The interfaces around each state are defined by the energy of the system minus the ground state energy. For B and I the interfaces are equally spaced from the state boundary by $1.5k_BT$ until the maximum possible energy is reached. The interfaces for the unbound state should be defined carefully. If one defines the interfaces based on the same energy spacing as for the bound states, particles could become stuck in a region where there is little binding energy and the system is subsequently not pushed towards the bound states as the transition is mostly entropic in nature. Therefore, we choose to define many interfaces close to the unbound state: $[10^{-6}, 10^{-5}, 10^{-4}, 10^{-3}, 10^{-2}, 10^{-1}, 0.4, 1.0]$. This choice of interfaces will guide towards the bound states.

TPT analysis

Although the full rate matrix K gives all kinetic information, the overall rate constant from B to U including the direct and indirect pathway via I can be calculated via TPT [110]. As given by Eq. 2.54, the commitment probability is the start of a TPT analysis. In this study there is only one intermediate state and therefore, the commitment probability for state I is simply given by:

$$q_I^+ = \frac{T_{IU}}{T_{IU} + T_{IB}} \tag{5.4}$$

where $T_{\mathcal{IJ}}$ is the transition probability to go from $\mathcal{I}$ to $\mathcal{J}$ in a certain lag time τ. From the committor we can calculate two interesting properties. Firstly, the overall rate constant for the dissociation process can be calculated explicitly:

$$k_{BU}^{TPT} = \frac{p_B T_{BU} + p_B T_{BI} q_I^+}{\tau(p_B + p_I q_I^-)} \tag{5.5}$$

where $p_{\mathcal{I}}$ is the equilibrium probability of state $\mathcal{I}$, and $q_{\mathcal{I}}^-$ is the backward-committor, $1 - q_{\mathcal{I}}^+$.

Secondly, the effective flux $f_{\mathcal{IJ}}$ gives frequency of a reactive pathway directly from B to U or indirectly B to U via an intermediate state I which can be generally calculated via Eq. 2.55. To calculate the net flux without any recrossings one computes: $f_{\mathcal{IJ}}^+ = \max[0, f_{\mathcal{IJ}} - f_{\mathcal{JI}}]$. For these simplified systems $f_{UB}^- = p_U T_{UB}$ and $f_{UIB}^- = p_U T_{UI} q_I^-$, where $q_I^- = 1 - q_I^+ = \frac{T_{IB}}{T_{IB}+T_{IU}}$.

Steady state approximation

We can also approximate the overall rate constant analytically by performing an analysis of the master equation: $\frac{dp_{\mathcal{I}}}{dt} = -\sum_{\mathcal{J}}^{M} p_{\mathcal{I}} k_{\mathcal{I}\mathcal{J}} + \sum_{\mathcal{J}}^{M} p_{\mathcal{J}} k_{\mathcal{J}\mathcal{I}}$ and assume a steady state approximation $\frac{dp_I}{dt} = 0$. This leads to an overall dissociation rate constant:

$$k_{BU}^{ss} = k_{BU} + \frac{k_{BI} k_{IU}}{k_{IB} + k_{IU}} \tag{5.6}$$

which is very similar to Eq. 5.5 if we use $k_{\mathcal{I}\mathcal{J}} = T_{\mathcal{I}\mathcal{J}}/\tau$, except for the term $p_I q_I^-$ in the denominator of Eq. 5.5 which drops out due to the assumption of a steady state where it is considered that $p_I << p_B$.

Simulation details

TIS simulations were performed with DMC in a periodic box of size $2r_U$. A production cycle of $5\text{x}10^5$ TIS cycles was performed after the scale factor for the Wang-Landau biasing was sufficiently low ($< 10^{-5}$), where every cycle consisted of 10 shooting, reversal, replica swap and state swap moves. Averages for the crossing probability and path densities were sampled after each move.

5.3 Results and discussion

We consider particles with narrow patches ($\delta = 10$ degrees) such that every bond is well defined and there are no multiple overlaps between patches. A small patch-width as used here was shown to reproduce the gas-liquid curves of protein solutions such as γ-crystallin and lysozyme quite well [138], albeit with more patches. From SRTIS we obtain the full rate matrix, $\mathbf{K}$, for each polyhedron which we show in Fig. 5.2 as a function of the patch-patch attraction, ϵ. Rate constants, k_{BU} and k_{IU} show clear Arrhenius behavior, *i.e.* $k_{\mathcal{I}\mathcal{J}} \propto \exp(-\beta \Delta G^{\dagger}_{\mathcal{I}\mathcal{J}})$, especially at high ϵ, where $\Delta G^{\dagger}_{\mathcal{I}\mathcal{J}}$ is the free energy barrier between $\mathcal{I}$ and $\mathcal{J}$. For low ϵ rate matrix elements k_{BI} and k_{IB} flatten off slightly, because these processes become more diffusion limited at very low ϵ. Naturally, the rate constant out of the bound state to the unbound state is lowest for the icosahedron as it has the highest number of bonds (Note that we compare here the situation for constant fixed patch interaction ϵ). For each polyhedron, the intermediate state has two bonds, and therefore each rate constant out of state I is very similar. Rate constants from k_{UB} and k_{UI} do not show Arrhenius behavior at all. Clearly, the rate limiting step in these types of transitions is the alignment of patches which is mostly a diffusive process.

Although the individual rate constants describe in principle the full association process, they are not intuitive. An interesting quantity for self-assembling systems is the overall rate constant which in part is responsible for the overall polyhedron yield. In Fig. 5.3 we show the overall association and dissociation rate constants as a function of total energy $E_{tot} = -n_b \epsilon$ to compare for equi-energetic clusters where we see that the overall rate constants are very much the same and there is

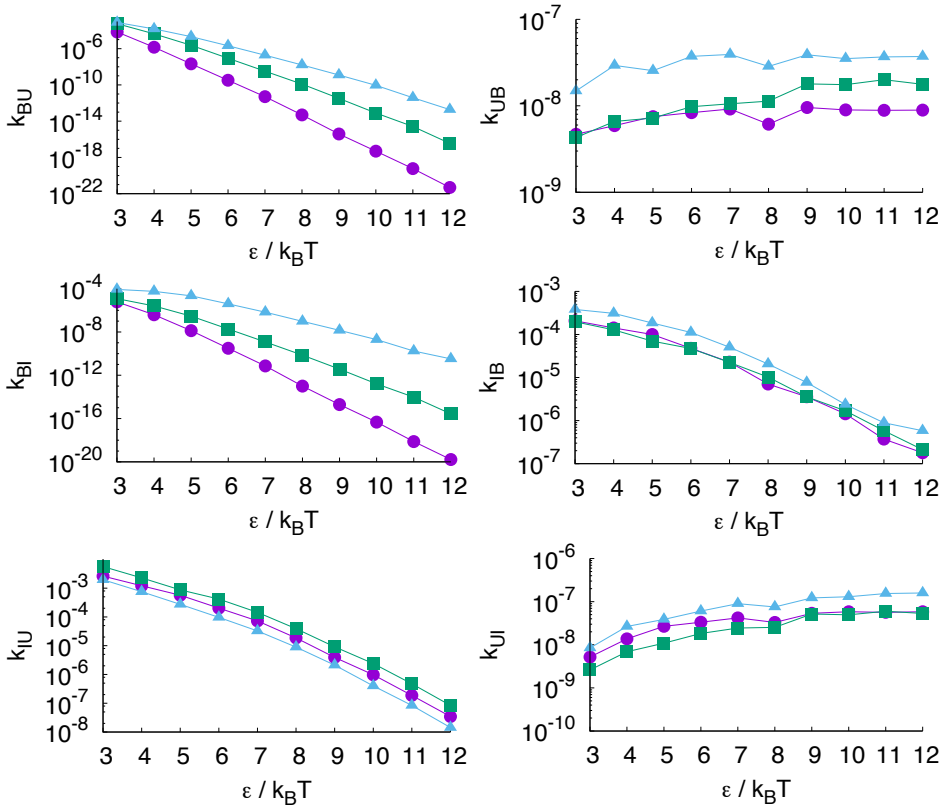

Figure 5.2: Rate matrix, K, for tetrahedron (light blue), octahedron (green) and icosahedron (purple) plotted as function of ϵ; k_{BU} (top left), k_{UB} (top right), k_{BI} (center left), k_{IB} (center right), k_{IU} (bottom left), k_{UI} (bottom right).

only a small difference between different polyhedra. The association rate constant of the tetrahedron differs from that of the octahedron and icosahedron, although this could be due to different volumes available to the unbound state and geometry of the system.

Clearly, the dissociation rate constant depends mostly on the total energy and is less dependent on the number of bonds or the intermediate states. This can be understood if we assume that two pathways contribute to the dissociation: direct dissociation from B to U and indirect dissociation via the intermediate state. As derived via steady state approximation in Eq. 5.6, the direct dissociation rate constant should be proportional to $k_+^{dir} \propto \exp(-n_b\epsilon)$ where n_b is the number of bonds of the system. The indirect dissociation could be approximated by the

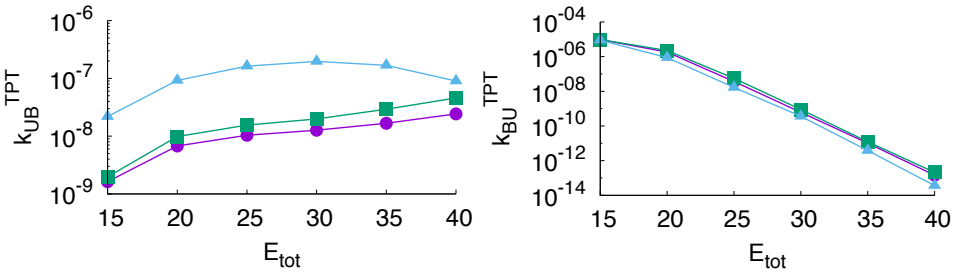

Figure 5.3: Effective association (left) and dissociation (right) rate constants calculated via TPT for the tetrahedron (blue triangles), octahedron (green squares) and icosahedron (purple circles). The effective association rate constants do not vary dramatically with the total energy. Differences can be attributed to the volume available to the unbound state, and the actual geometry of the cluster. Effective dissociation rate constants do depend on the total energy following roughly the Arrhenius law (except at low binding energy), and do not differ much between polyhedra for the same total energy

steady state solution: $k_+^{ind} = k_{IU}k_{BI}/(k_{IB} + k_{IU})$. Based on simple fits to the Arrhenius relation from Fig. 5.2 the following relations should approximately hold: $k_{IU} \propto \exp(-2\epsilon)$, $k_{BI} \propto \exp(-(n_b-1)\epsilon)$, $k_{IB} \propto \exp(-\epsilon)$. The steady state solution becomes:

$$k_+^{ind} = \frac{\exp(-(n_b+1)\epsilon)}{\exp(-\epsilon) + \exp(-2\epsilon)} \tag{5.7}$$

if we further approximate that $\exp(-\epsilon) \gg \exp(-2\epsilon)$ which is valid for high ϵ, the dissociation rate constant for every polyhedron becomes $k_+ = \exp(-n_b\epsilon)$. Therefore, as shown by Fig. 5.3 the total dissociation rate constant, k_{BU}^{TPT}, is mostly dependent on the total energy given by $E_{tot} = -n_b\epsilon$. Vibrational and rotational entropy naturally also plays a role, however, it seems less significant especially at high patch attraction. Although it seems fairly trivial, this does mean that apparently the number of bonds a particle is bound to does not make a difference if we compare the same total energy. Note that the result would be the same if state I has a different number of bonds.

Although the rate constants are not different, the mechanism of assembly or disassembly can be different, which in turn impacts the overall assembly. If a system resides longer in the intermediate state, frustrated dangling bonds can lead to kinetically trapped states, when other particles from the bulk attach to a growing structure. Moreover, if during assembly intermediate states are frequently visited, the probability of trapping naturally also increases. More information about the mechanism can be distilled from the TPT analysis. For comparison we plot the ratio f_{UIB}/f_{UB} in Fig. 5.4. This ratio demonstrates whether the direct or the in-

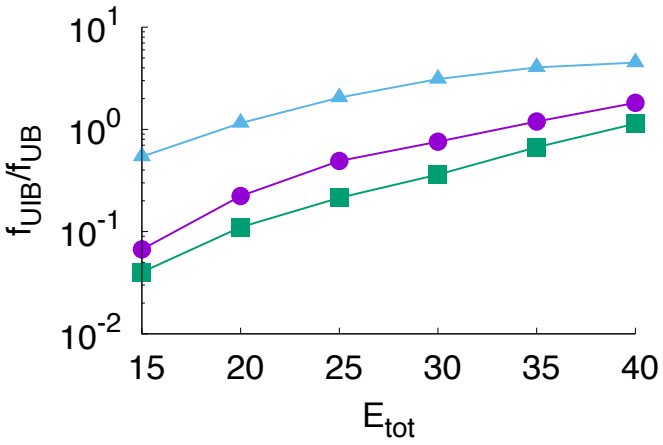

Figure 5.4: Ratio of the flux from the unbound state indirectly via the intermediate state to the bound state over the flux directly to the bound state for the tetrahedron (blue triangles), octahedron (green squares) and icosahedron (purple circles), indicating, surprisingly, that the octahedron visits the intermediate state least frequently.

direct pathway is dominant in the equilibrium association process. An interesting observation is that the octahedron has the lowest flux via the intermediate state and the tetrahedron the highest. Despite the lower individual patch strength, the intermediate state of the icosahedron is visited more often than the octahedron. This might be due to the fact that there exist many more distinct but identical intermediate states for the icosahedron ($N_{int} = 50$) than for the octahedron ($N_{int} = 16$), which increases the accessibility of the intermediate state for the icosahedron, and therefore also the frequency of visiting the intermediate state.

Another way of analyzing the rate matrix is by monitoring the relaxation of the populations towards equilibrium, which reflects the residence time in intermediate states. In Fig. 5.5 the relaxation of the population ratio P_I/P_B is shown for $\epsilon = 10k_BT$ where clearly, the icosahedron state has the highest population in the intermediate state and tetrahedron the lowest. Therefore, if we compare with equal patch strength, the icosahedron resides the longest in the intermediate state. However, again it makes for a better comparison if the systems are not compared

via equal patch strength, but equal total energy. In Fig. 5.6 the relaxation of the

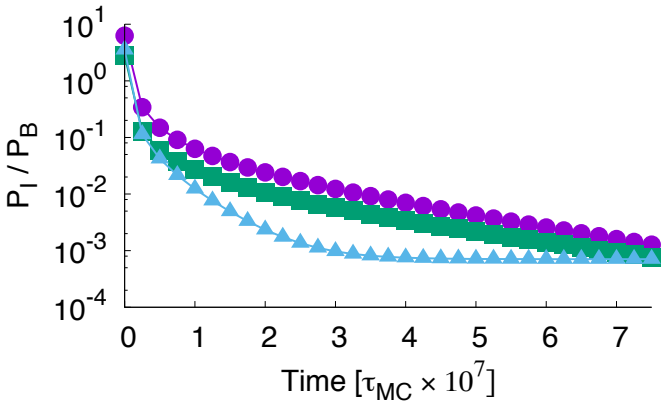

Figure 5.5: Ratio of the intermediate population over the bound state relaxing from the unbound state for the tetrahedron (blue triangles), octahedron (green squares) and icosahedron (purple circles) for a fixed bond strenght $\epsilon = 10k_BT$ demonstrating that the icosahedron is relatively the longest in the intermediate state. Note that the order is different than for the f_{UIB}/f_{UB} shown in Fig. 5.4, demonstrating that there is a difference between the equilibrium net-flux and the out-of-equilibrium relaxation pathways.

population ratio P_I/P_B is shown for $E_{tot} = -40k_BT$ which demonstrates that the tetrahedron state clearly has relatively the highest population in the intermediate state when the systems are compared with equal total energy. Note that for all three systems the population of the bound state is almost unity and that the full relaxation is not shown. The ordering is different than for the f_{UIB}/f_{UB} shown in Fig. 5.4, demonstrating that there is a difference between the equilibrium net flux and the out-of-equilibrium relaxation pathways. Moreover there is a clear difference between the frequency of visiting intermediate states, as predicted by TPT analysis, and the dwell time in the intermediate state, which is important for the population dynamics.

From the SRTIS path ensemble we can also extract the mechanism of self-assembly and dissociation by projecting reactive pathways on collective variables. Here we focus on the dissociation pathways from the bound state B. The reactive path density is defined as in Eqn. 2.52:

$$n_B^r(\mathbf{q}) = \int \mathcal{D}\mathbf{x}^L \mathcal{P}_B^r[\mathbf{x}^L] h_{\mathbf{q}}(\mathbf{x}^L). \tag{5.8}$$

where $\mathcal{D}\mathbf{x}^L$ is a proper integral over all pathways, $\mathcal{P}_B^r[\mathbf{x}^L]$ is the probability of a reactive pathway out of state B and $\mathbf{q}(\mathbf{x}_k)$ is the collective variable of choice. In Fig. 5.7 we show the reactive path density for dissociation from state B mapped onto the distance of the motile particle to the polyhedral cluster, R and total

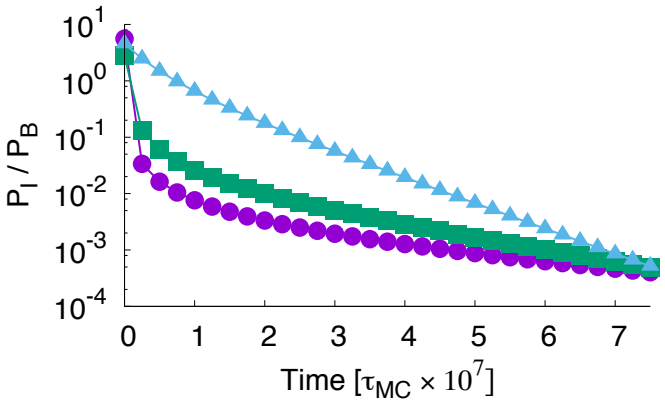

Figure 5.6: Ratio of the intermediate population over the bound state relaxing from the unbound state for $E_{tot} = -40k_BT$ demonstrating that the tetrahedron stays the longest time in the intermediate state, due to the fact that it is harder to break a bond in the tetramer than in the octahedron or icosahedron.

energy, E_{tot}. Clearly, in case of the tetrahedron reactive pathways from B are dominated by the $B \to I$ transition. This is a reflection of Fig. 5.4 that shows that the intermediate frustrated state is frequented often during the (dis)assembly of a tetrahedron complex. In contrast, the intermediate state is mostly avoided for the octahedron and icosahedron, where clearly the highest probability follows the $B \to U$ transition. Note also that the path probability from $B \to I$ is indeed slightly higher for the icosahedron than for the octahedron as indicated by Fig. 5.4.

Conclusions

We studied the effect of multivalency on the kinetics and mechanism of self-assembly of patchy particles forming polyhedral clusters. By using SRTIS we were able to obtain the complete rate matrix and thus the full kinetic picture of these simple patchy particle systems. No difference in kinetics is found when the total energy of the ground-state is fixed which corroborates with a simple steady state analysis. In contrast, the mechanism of self-assembly does depend on the properties of the intermediate state. All studied multivalent particles system can associate into a metastable intermediate state, in which two bonds are formed, and the others are not. From this intermediate state the system can relax into the correctly formed fully bound state. Pathways that visit the intermediate states are less prevalent for five-fold multivalent particles compared to particles with only three bonds. Instead the association pathways are more likely to navigate directly from unbound to bound without visiting the intermediate states. Long sojourns in the intermediate state can lead to kinetic trapping, and malformed aggregates.

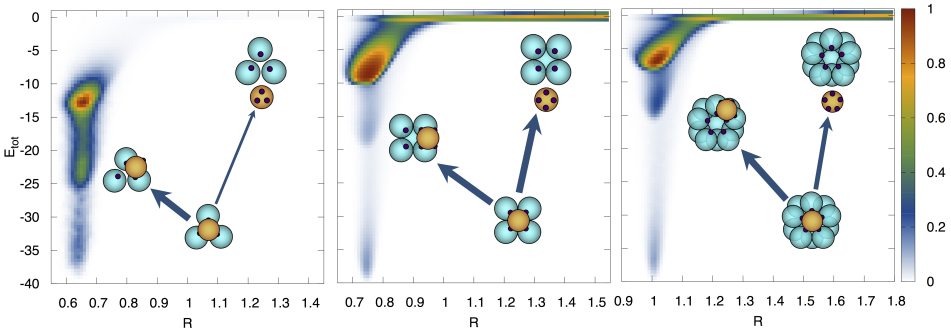

Figure 5.7: Reactive path density obtained from the reweighted path ensemble, representing the dissociation mechanism starting from correctly bound state B. The path density is mapped onto the distance, R, between the motile particle and the polyhedral cluster and the binding total energy, E_{tot}. For the tetrahedron (left), the most dominant escape from the bound state, located at $E_{tot} = -40k_BT$ ends up via diffusion in the one bond state located for the tetrahedron at $E_{tot} = -13.3k_BT$, in state I located at $E_{tot} = -26k_BT$. Clearly, direct dissociation to the unbound state is not very probable. In contrast, escape from B for the octahedron (middle) and icosahedron (right) clearly does end up in U and not only in the frustrated state I. Moreover, the icosahedron shows to have more reactive path probability to the I state than the octahedron which is also reflected in the flux ratio f_{UIB}/f_{UB} in Fig. 5.4. Note that due to microscopic reversibility this analysis also holds for assembly, rather than disassembly.

It is therefore kinetically favorable for self-assembling systems to have a ground state where particles form many bonds which stabilize the ground state instead of only a few which would result in strongly frustrated intermediate states.

Furthermore, we found a difference between the equilibrium net-flux and the out-of-equilibrium relaxation pathways. In the net flux analysis, long sojourns in intermediate states are not taken into account, simply only the number of times a certain state is visited along (dis)assembly. The number of times a state is visited of course does not necessarily depend on the stability of this state, but on the kinetic accessibility of the state which depends on the number of microstates a macrostate entails. The icosahedron has more microstates in I (50) than the octahedron (16). This difference is also reflected in the net flux ratio.

Although the studied systems are too simple to represent real proteins or even colloidal particles, some general observations about self-assembly of complexes can be made. The generic conclusion that particles with many weak bonds in the ground state are able to self-assemble in a more defect-free way than particles with a few strong bonds, might be interesting for the experimental design of colloid particles to form desired structures. While our evidence is restricted to the symmetry cases that we used here (tetrahedron, octahedron, icosahedron) we speculate that

other symmetries also show similar features. Our general conclusion implies that natural occurring systems that spontaneously form complex structures with high fidelity from multivalent particles such as virus shells, would show a tendency to have more rather less binding sites.

Naturally, it would be even more informative to study the full unrestricted dynamics of particles for these different type of clusters, i.e. to investigate the assembly pathways starting from 12 unbound particles in case of the icosahedron. However, with increasing motility also comes an exponentially increasing number of intermediate states which might become intractable. An adaptive scheme can be considered to automatically find only the important intermediate states such as adaptive TIS or a Markov State Model [71, 104].